

Supplementary Materials for

**Translesion DNA synthesis mediates acquired resistance to olaparib plus temozolomide in small cell lung cancer**

Marcello Stanzione, Jun Zhong, Edmond Wong, Thomas J. LaSalle, Jillian F. Wise, Antoine Simoneau, David T. Myers, Sarah Phat, Moshe Sade-Feldman, Michael S. Lawrence, M. Kyle Hadden, Lee Zou, Anna F. Farago, Nicholas J. Dyson\*, Benjamin J. Drapkin\*

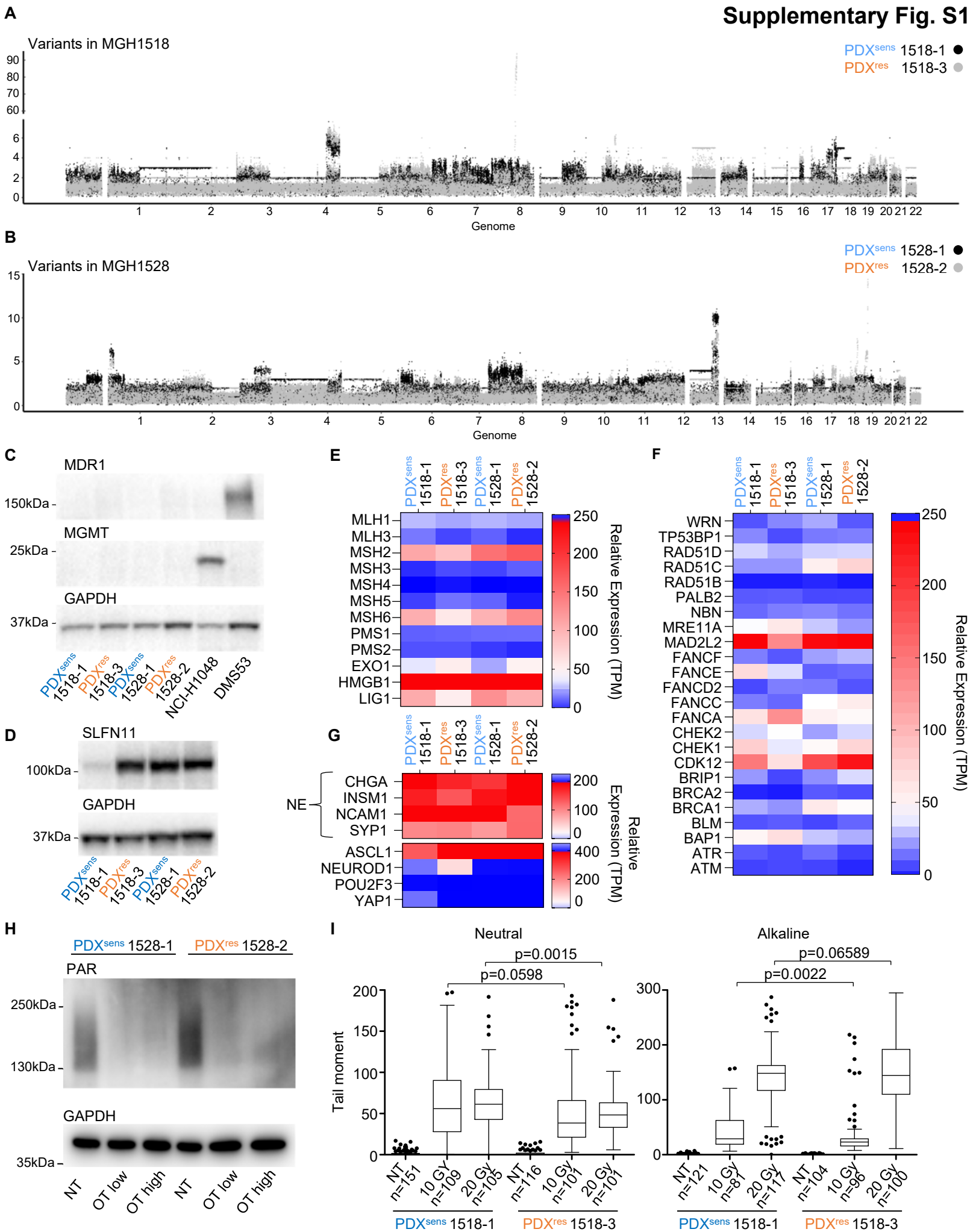
\*Corresponding author. Email: benjamin.drapkin@utsouthwestern.edu (B.J.D.);  
dyson@helix.mgh.harvard.edu (N.J.D.)

Published 13 May 2022, *Sci. Adv.* **8**, eabn1229 (2022)  
DOI: 10.1126/sciadv.abn1229

**This PDF file includes:**

Figs. S1 to S9

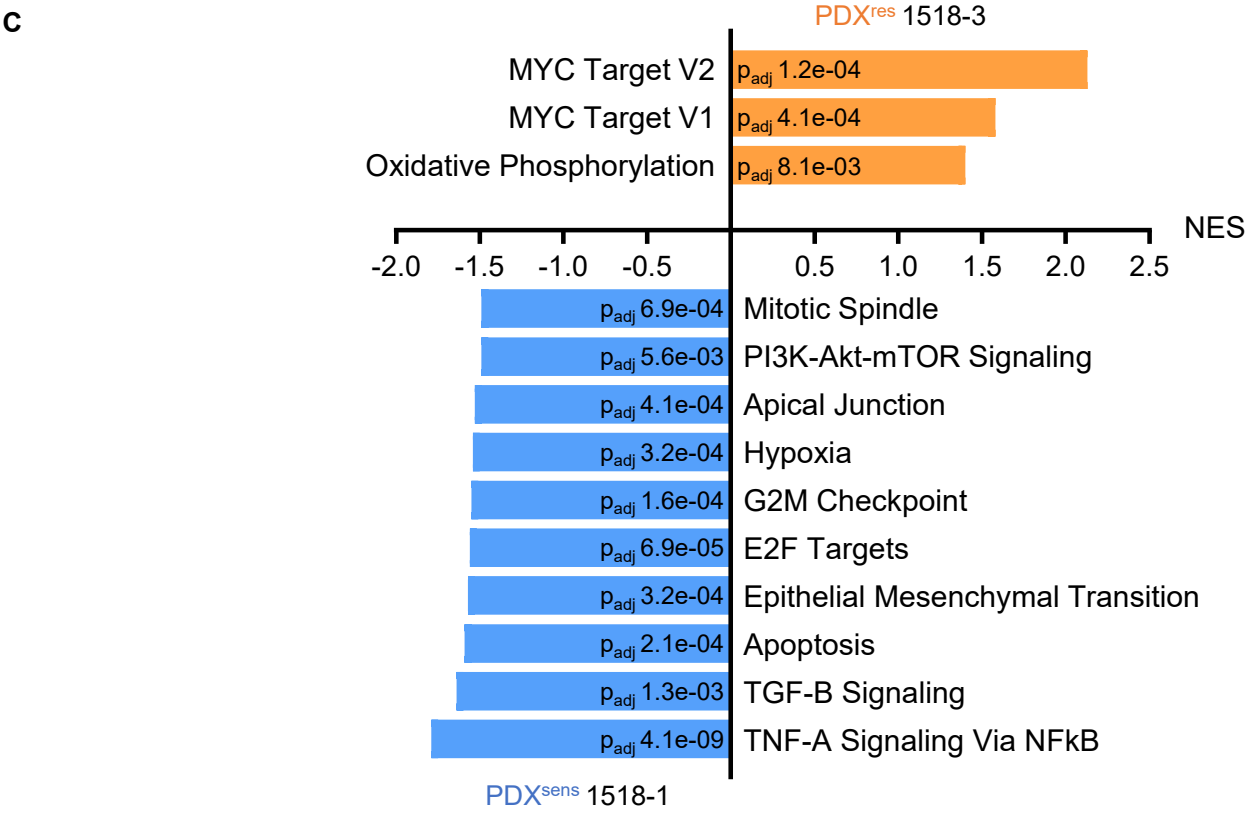
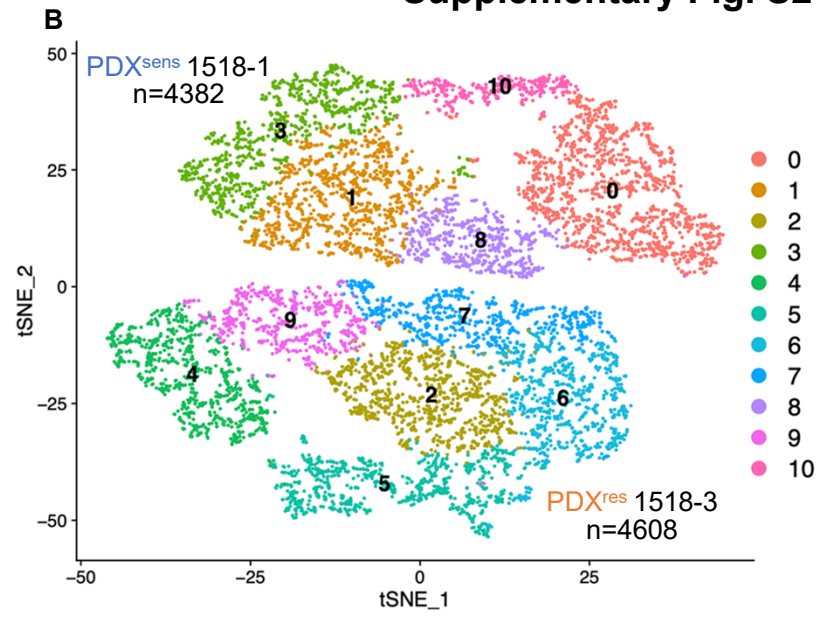
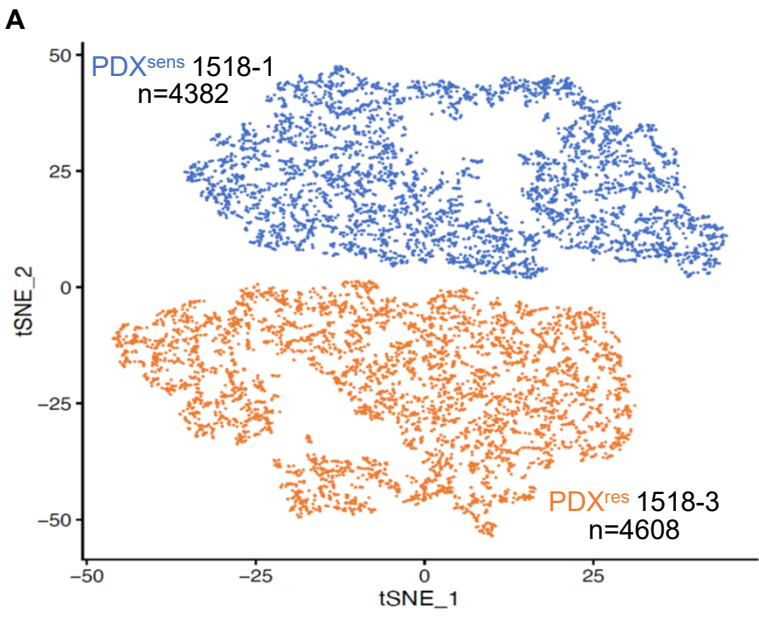
References



## Supplementary Fig. S1

### Genomic alterations and expression of common chemoresistance markers in PDX serial models.

(A, B) Genome-wide plots of the identified somatic variants and their adjusted variant allele frequency, Adjusted VAF was calculated for each somatic variant by multiplying by the copy state of the genomic region. (C, D) Western-blot analysis of protein extracts from untreated xenograft tissue lysates. Analyzed PDX models are indicated. MDR1, MGMT and SLFN11 were detected and GAPDH was used as loading control. Protein extracts from lysates of NCI-H1048 and DMS53 SCLC cell lines were used as positive controls. (E, F, G) Heat map showing the mRNA abundance (transcripts per million, TPM) of known components of the DNA mismatch repair (MMR) pathway (E), BRCAness signature associated factors (83) (F) and markers of SCLC neuroendocrine status (CHGA, INSM1, NCAM1 and SYP1) or SCLC molecular subtypes (ASCL1, NEUROD1, POU2F3 and YAP1) (G); NE indicates neuroendocrine status. We did not observe any significant variation in the expression of genes involved in MMR, BRCAness pathway, NE status or changes in molecular subtype in both resistant samples. (H) Western-blot analysis of protein extracts from isolated tumor cells. Total protein PARylation (PAR) was detected and GAPDH was used as loading control. Two treatment regimens were used: OT low (Olaparib 0.25 $\mu$ M + TMZ 35 $\mu$ M) and OT high (Olaparib 0.5 $\mu$ M + TMZ 70 $\mu$ M). NT indicates not treated samples. (I) DNA damage assessment after  $\gamma$ -irradiation of tumor cells isolated from freshly dissected SCLC PDXs. Two  $\gamma$ -irradiation regimens were used, 10 and 20 Gray (Gy), and NT indicates not treated samples. Quantification of the comet tail moment (% of DNA in the tail multiplied by the distance between means of the head and tail distributions) is shown. Box-plots represent interquartile ranges, horizontal lines denote the median and points indicate outliers. Statistical significance calculated by two-tailed Mann–Whitney test. Two independent experiments were performed and numbers of quantified comets from one representative experiment are shown.

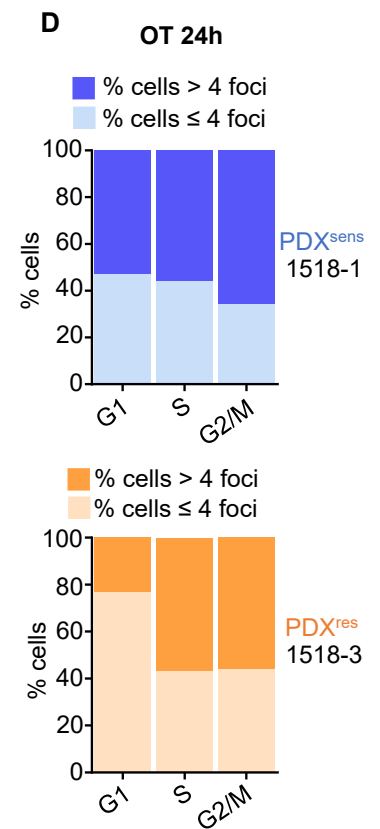
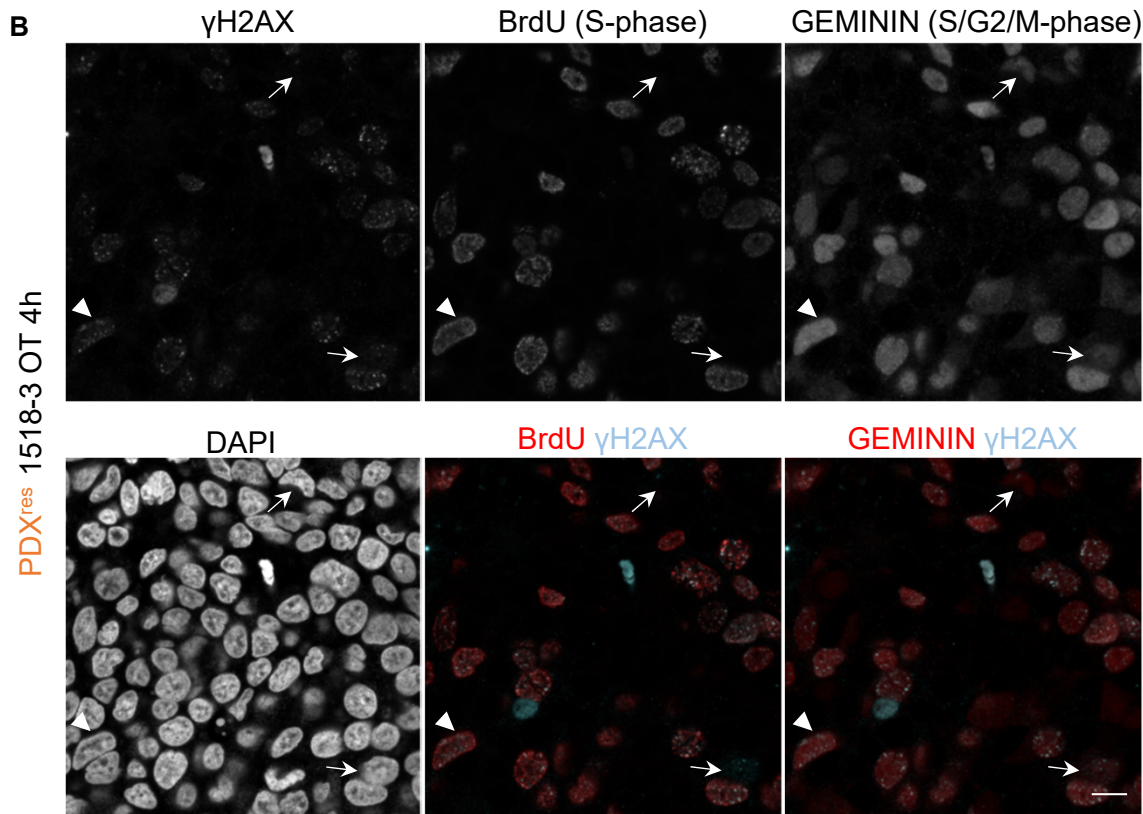
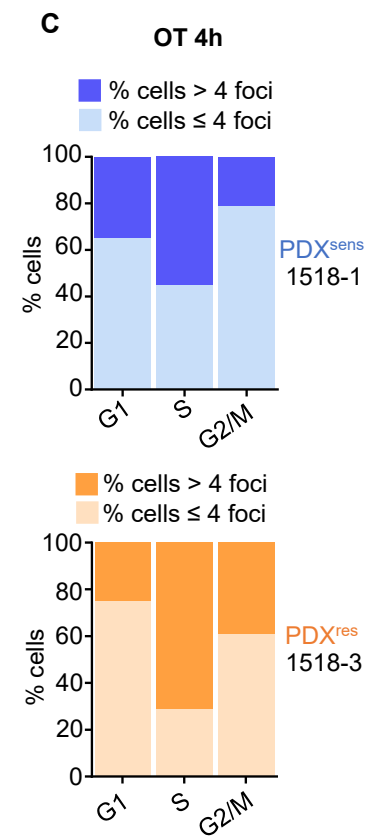
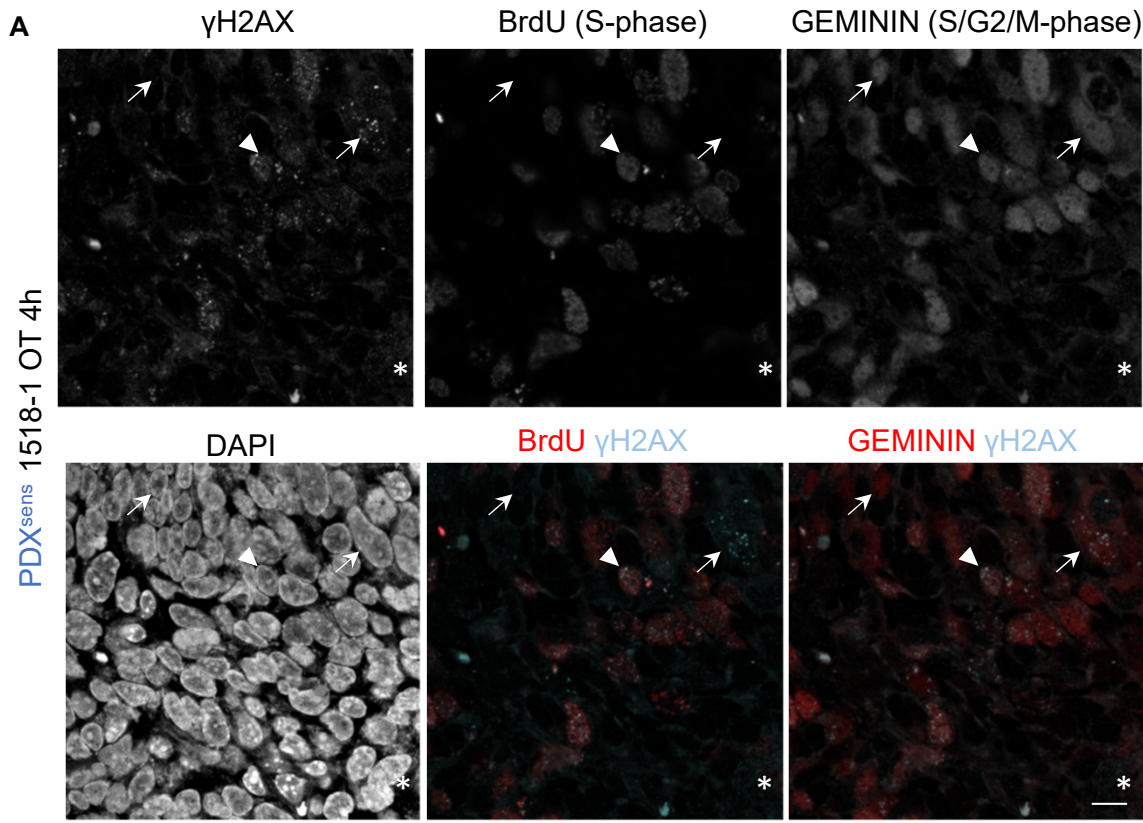


## Supplementary Fig. S2

### Single cell RNA sequencing analysis of PDX<sup>sens</sup> 1518-1 and PDX<sup>res</sup> 1518-3.

(**A, B**) tSNE plots displaying single-cell RNA-seq data of the indicated SCLC models. Each dot corresponds to a single analyzed cell, and total number of analyzed cells is indicated. Seurat clustering is shown in **B** using a resolution of 0.7. Data suggest that PDX<sup>sens</sup> 1518-1 and PDX<sup>res</sup> 1518-3 tumors are transcriptionally distinct and none of the identified subpopulations are overlapping between models. (**C**) Gene set enrichment analysis for Hallmark gene sets from MSigDB showing significant enrichment in the differential gene expression result between PDX<sup>sens</sup> 1518-1 and PDX<sup>res</sup> 1518-3. Bar lengths correspond to normalized enrichment score (NES), with positive NES values indicating enrichment in PDX<sup>res</sup> 1518-3 and negative values indicating enrichment in PDX<sup>sens</sup> 1518-1. p-adj values shown within each column denote significance levels after p values correction with the Benjamini-Hochberg procedure.

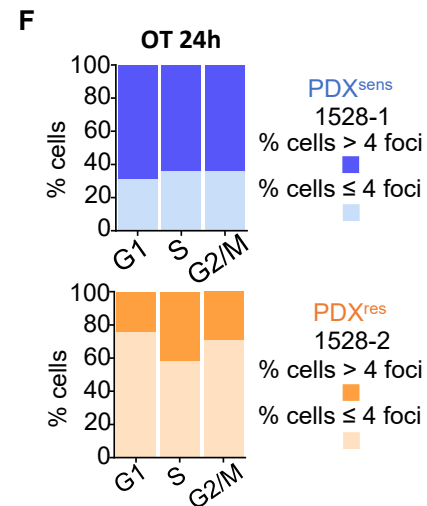
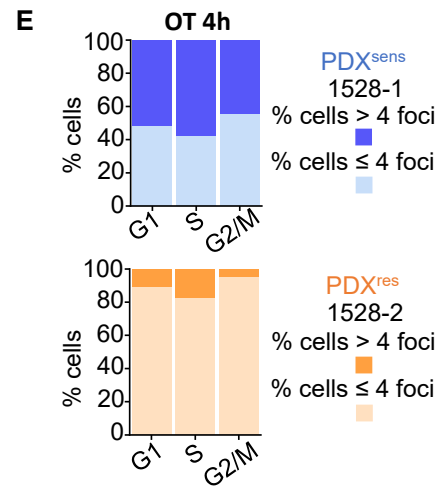
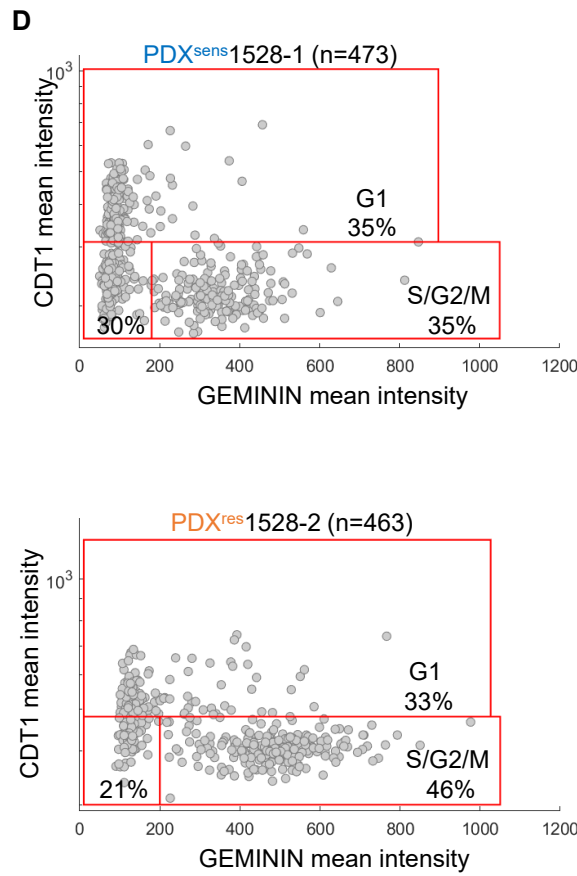
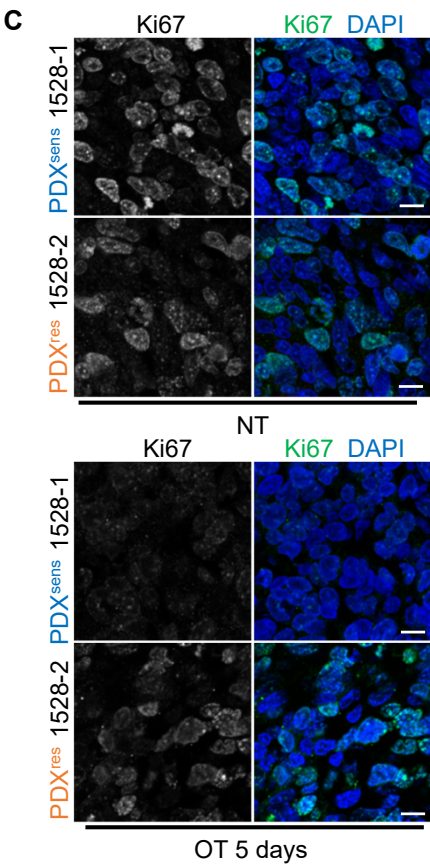
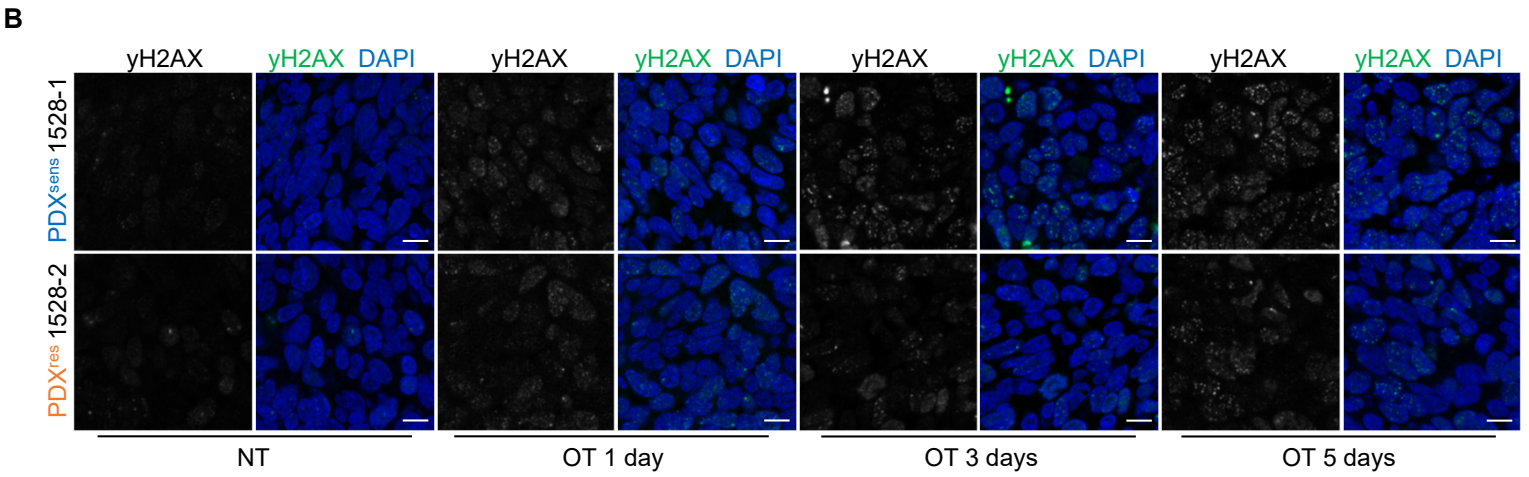
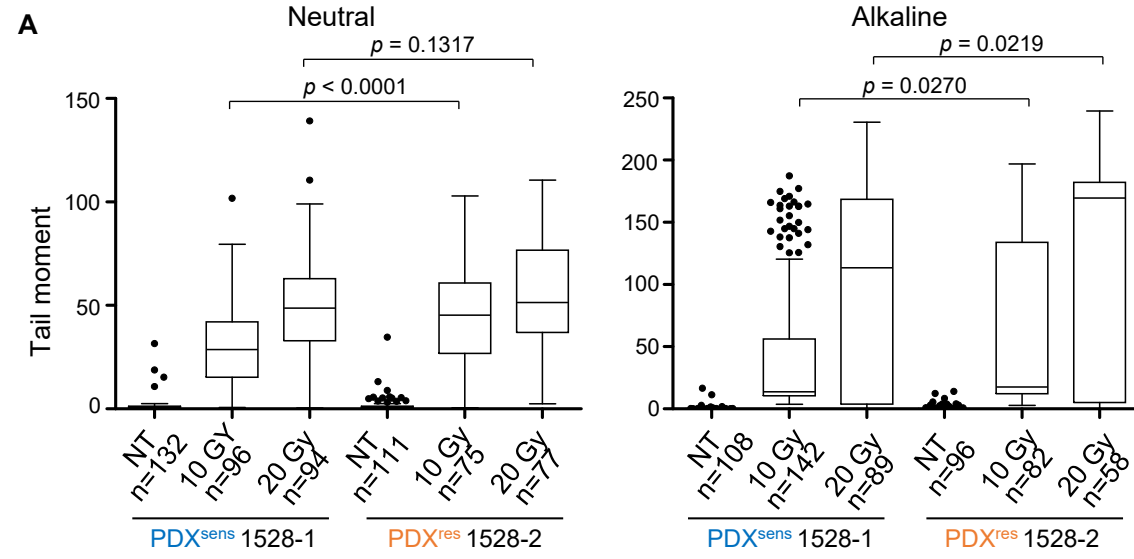
# Supplementary Fig. S3



### Supplementary Fig. S3

Cell cycle and OT-induced DNA damage analysis in PDX<sup>sens</sup> 1518-1 and PDX<sup>res</sup> 1518-3.

(A, B) BrdU, GEMININ and  $\gamma$ H2AX were immunodetected on xenograft tissue sections of the indicated models 4 hours post OT treatment. Nuclei were detected by DAPI, bars are 20 $\mu$ m. White arrows indicate GEMININ positive, BrdU negative tumor cells (G2/M phase); white arrowheads indicate GEMININ-BrdU double positive tumor cells (S phase); white asterisks indicate GEMININ-BrdU double negative tumor cells (G1 phase). (C, D) Bar graphs show the percentage of cells with  $\leq$  or  $>$  than 4  $\gamma$ H2AX foci in each cell cycle phase as determined by GEMININ-BrdU- $\gamma$ H2AX staining 4 hours (C) or 24 hours (D) after OT treatment in the indicated PDX models.



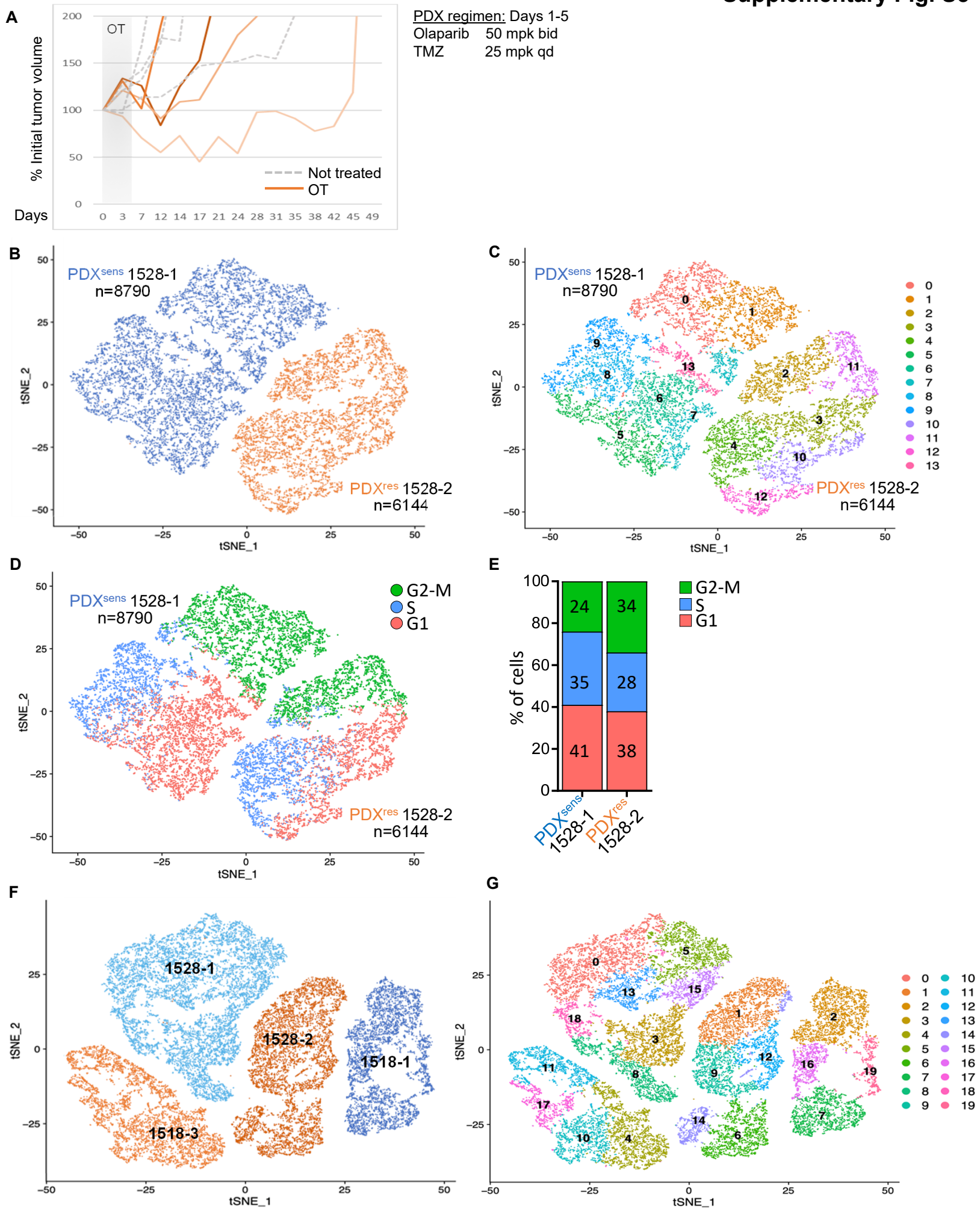


## Supplementary Fig. S4

### Different acquired chemoresistance mechanism in PDX<sup>res</sup> 1528-2.

(A) DNA damage assessment after  $\gamma$ -irradiation of tumor cells isolated from freshly dissected SCLC PDXs. Two  $\gamma$ -irradiation regimens were used, 10 and 20 Gray (Gy), and NT indicates not treated samples. Quantification of the comet tail moment (% of DNA in the tail multiplied by the distance between means of the head and tail distributions) is shown. Box-plots represent interquartile ranges, horizontal lines denote the median and points indicate outliers. Statistical significance calculated by two-tailed Mann–Whitney test. Two independent experiments were performed and numbers of quantified comets from one representative experiment are shown. (B, C)  $\gamma$ H2AX (B) or Ki67 (C) were immunodetected on xenograft tissue sections and nuclei were detected by DAPI. Bars, 10 $\mu$ m. (D) CDT1 (G1 phase marker) and GEMININ (S-G2-M phase marker) were immunodetected on tumor tissue sections of the indicated models and nuclei were detected by DAPI (images not shown). Plots show the mean fluorescence intensity of both CDT1 and GEMININ for each cell represented by a gray dot and percentage of cells in the specific cell cycle phase are shown. (E, F) Bar graphs show the percentage of cells with  $\leq$  or  $>$  than 4  $\gamma$ H2AX foci in each cell cycle phase as determined by GEMININ-BrdU- $\gamma$ H2AX staining 4 hours (E) or 24 hours (F) after OT treatment in the indicated PDX models.

OT treatment response 1528-2 post-5dOT

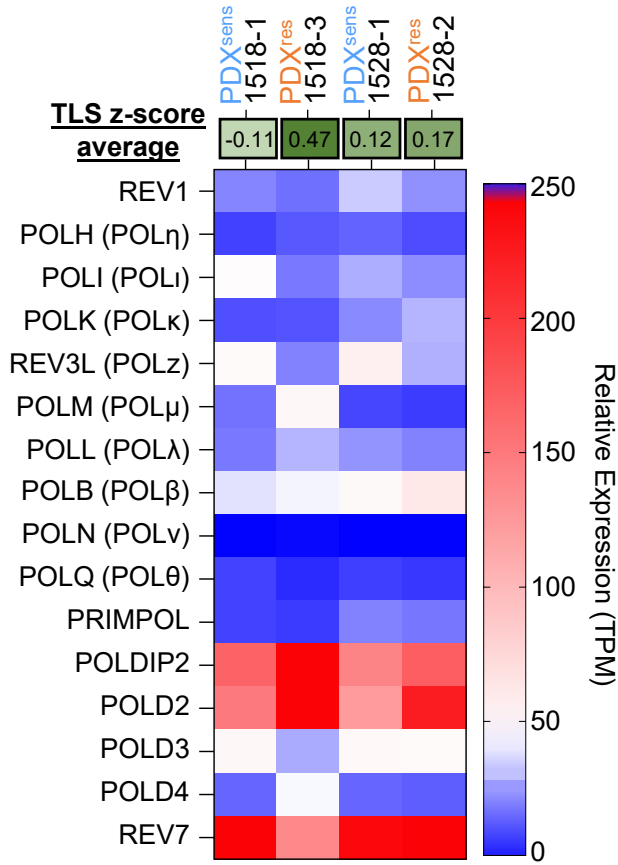


## Supplementary Fig. S5

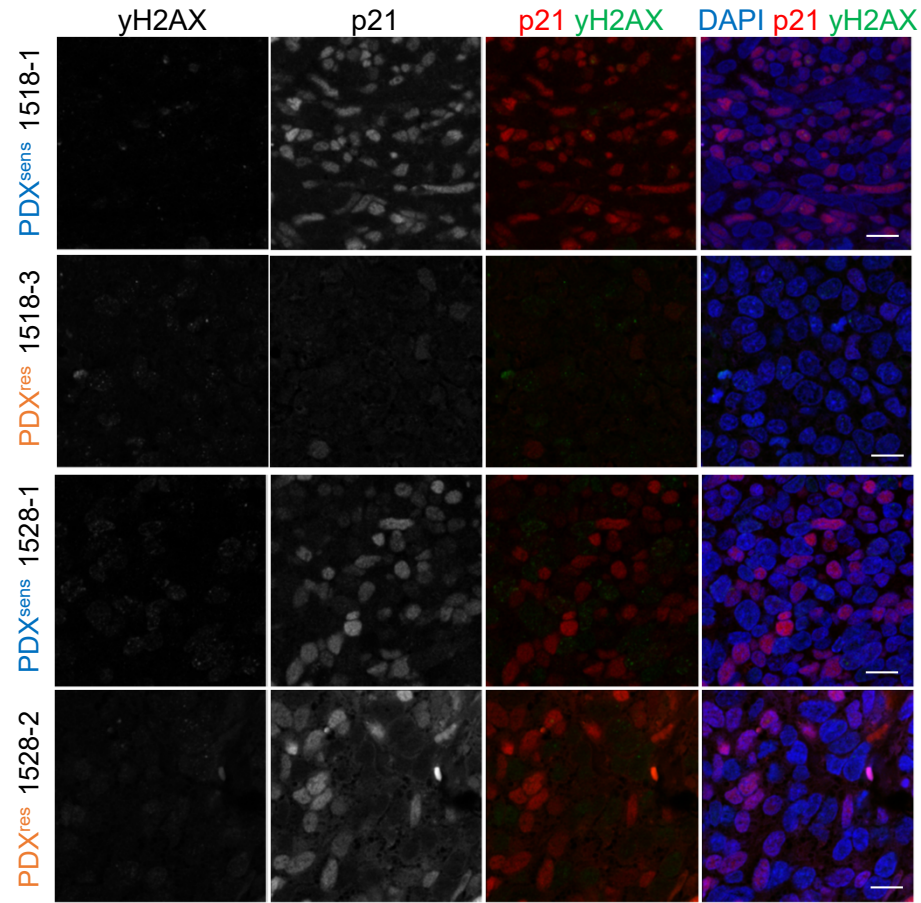
### Single cell RNA sequencing analysis of PDX<sup>sens</sup> 1528-1 and PDX<sup>res</sup> 1528-2.

(A) Tumor volume curves represent % initial tumor volume versus time (days) after a single cycle of OT (OT treatment regimen is indicated). Tumor volume curves for untreated xenografts are in gray dashed lines, curves for OT treated xenografts are in orange solid lines. 4 replicate xenografts are plotted for each treatment. Grayed area represents the treatment cycle. (B-C and F-G) tSNE plots displaying single-cell RNA-seq data of the indicated SCLC models. Each point corresponds to a single analyzed cell, and the total number of analyzed cells is indicated. Seurat clustering is showed in C and G using resolutions of 0.7 and 1, respectively. Data suggest that PDX<sup>sens</sup> 1528-1 and PDX<sup>res</sup> 1528-2 tumors are transcriptionally distinct and none of the identified subpopulations are overlapping between models. (D-E) tSNE plot showing the predicted cell cycle phase of each analyzed cell from the two MGH1528 models. Each point represents a tumor cell. Prediction was performed using the Seurat CellCycleScoring package, and percentage of cell in each cell cycle phase are shown in E. (F-G) tSNE plots displaying single-cell RNA-seq data of the indicated SCLC models. The data here suggest that the clustering of cells derived from these 4 serial models is primarily driven by the patient of origin and resistance status (intertumoral heterogeneity).

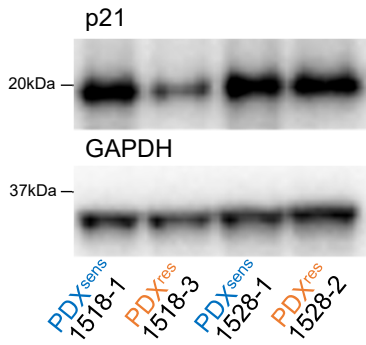
A



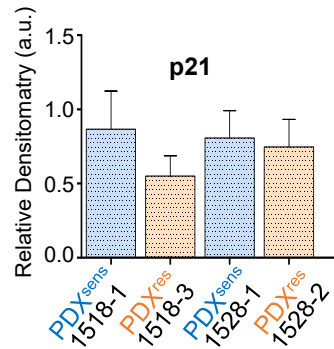
B



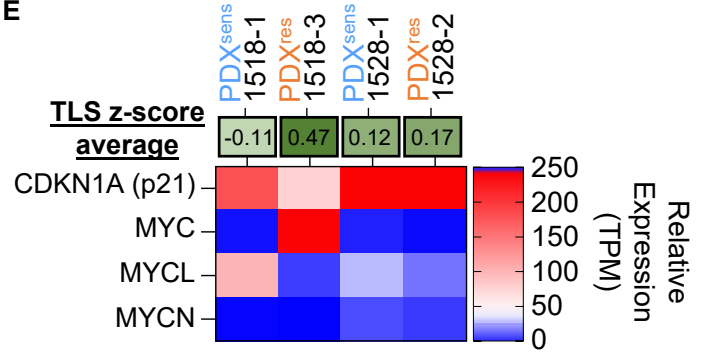
C



D



E

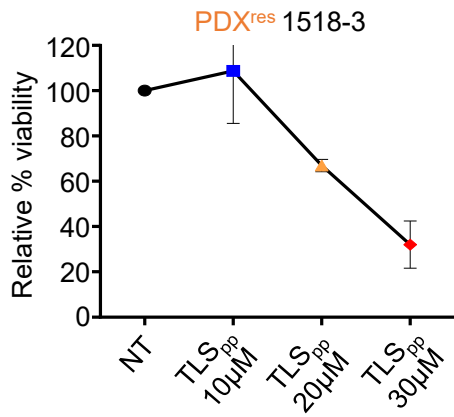


## Supplementary Fig. S6

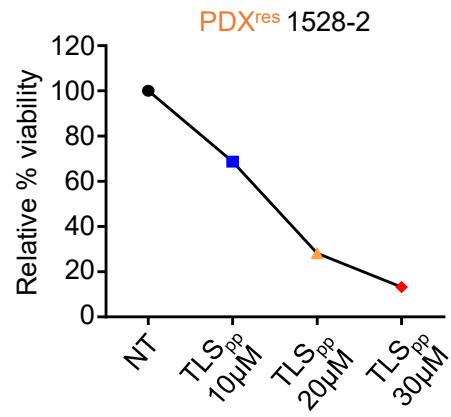
### Expression of TLS pathway components in SCLC PDX<sup>sens</sup> and PDX<sup>res</sup>.

(A) Heat map showing the mRNA abundance (transcripts per million, TPM) of known translesion DNA synthesis (TLS) components. The average “TLS z-score”, shown in the top row, was calculated as the average of the z-scores obtained for each transcript of the signature for each model against the panel of SCLC PDXs previously tested for OT sensitivity(25). (B)  $\gamma$ H2AX and p21 were immunodetected on xenograft tissue sections of the indicated PDX models and nuclei were detected by DAPI. Bars, 10 $\mu$ m. (C) Western-blot analysis of protein extracts from xenograft tissue lysates. p21 was detected in samples from the indicated PDX models and GAPDH was used as loading control. (D) Plot shows quantification of p21 protein levels in the indicated samples by quantitative densitometry. Densitometry was performed on each band, background was subtracted, and ratios of each protein to the GAPDH loading control were calculated. The plot shows the results from three independent experiment. (E) Heat map showing the mRNA abundance (transcripts per million, TPM) of CDKN1A (p21), MYC, MYCL and MYCN in the indicated PDX models. The average “TLS z-score” shown in the top row is the same as in A.

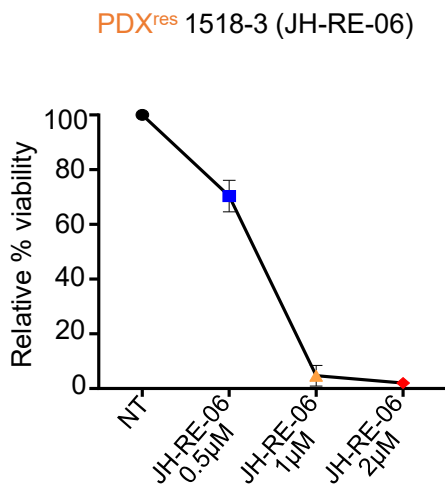
A



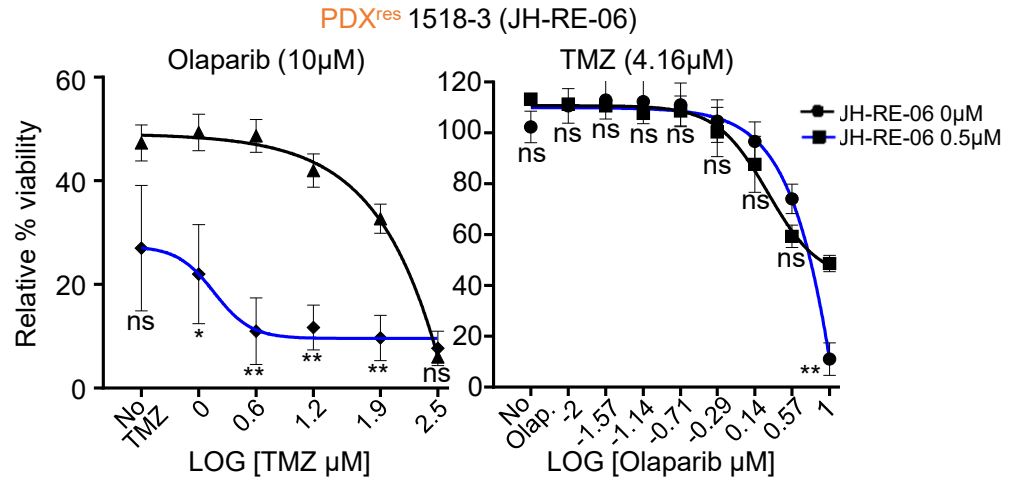
B



C



D



### Supplementary Fig. S7

TLS inhibition synergize with OT treatment and increase its efficacy in SCLC cells isolated from PDXs.

(A-C) Graphs show cell viability in the presence of different concentrations of TLS<sub>pp</sub> (A-B) or JH-RE-06 (C). Drug concentration and tested cell types are indicated. Data represent the mean percentages of survival from at least two independent experiments. (D) Cell survival assay with PDX<sup>res</sup> 1518-3 cells treated with OT at indicated concentrations, in the presence of JH-RE-06 (blue curve) or without JH-RE-06 (black curve). Synergy data obtained using JH-RE-06 1 $\mu$ M and 2 $\mu$ M were uninformative because of high sensitivity to JH-RE-06 single agent.

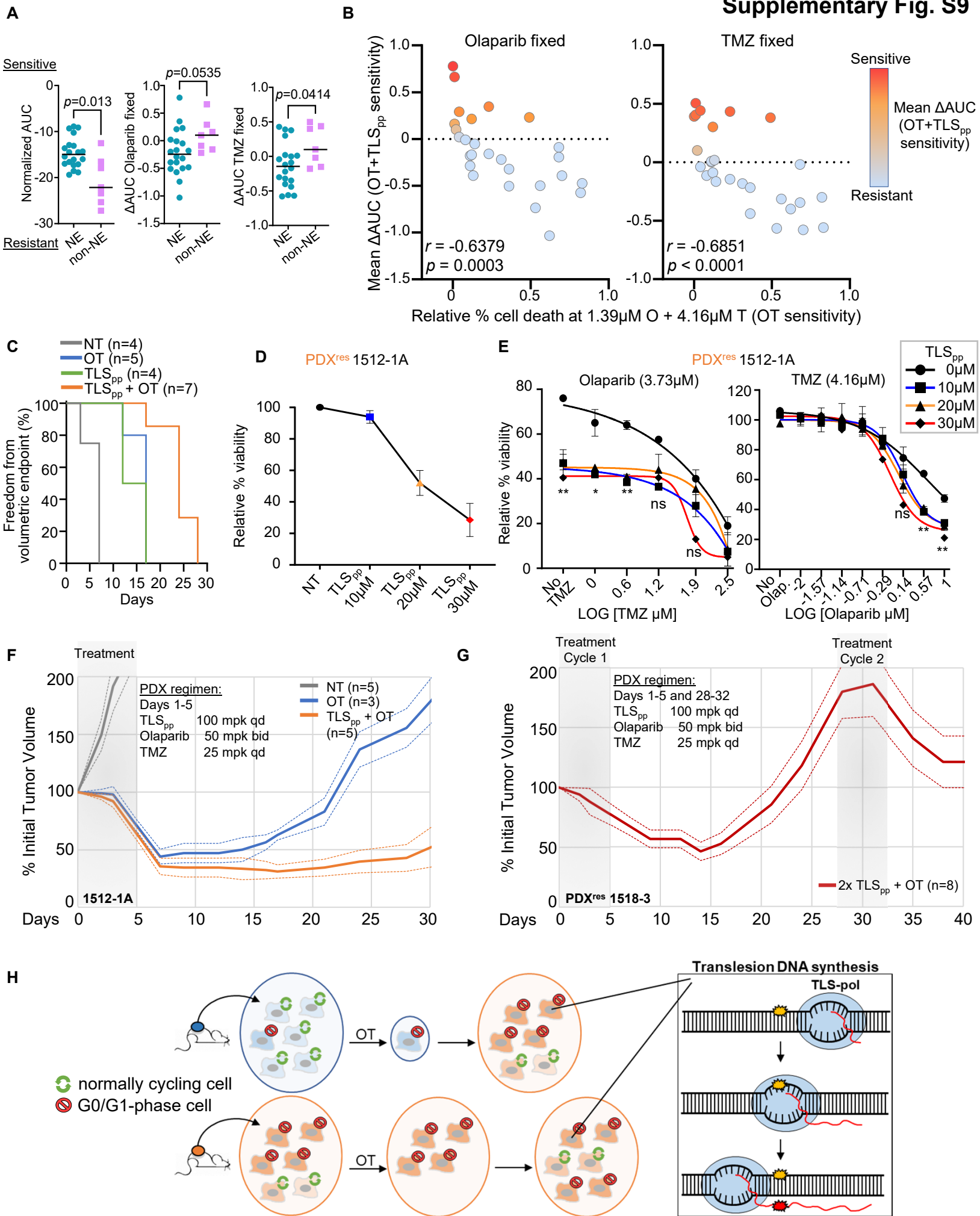




## Supplementary Fig. S8

TLS inhibition synergize with OT treatment and increase its efficacy in SCLC established cell lines.

(A) Explanatory legend for the AUC (area under the curve) values used to create the heatmap showed in Fig. 7C. (B) Explanatory legend for the  $\Delta$ AUC ( $\Delta$  area under the curve) values used to create the heatmap showed in Fig. 7D. (C-H) Cell survival assays with either U2OS (C), DMS114 (D), NCI-H2029 (E), NCI-H526 (F), NCI-H841 (G) or DMS53 cells (H) treated with OT at indicated concentrations, in the presence of TLS<sub>pp</sub> (gray, blue, orange, and red curves) or without TLS<sub>pp</sub> (black curve). Left panels show cell viability when treated with fixed concentration of olaparib and increasing concentration of TMZ. Right panels show cell viability when treated with fixed concentration of TMZ and increasing concentration of olaparib. Data represent the mean percentages of survival from at least two independent experiments. Statistical analysis was calculated with one-way ANOVA Tukey multiple comparisons and all P values are described in the section "Statistical methods".



## Supplementary Fig. S9

OT + TLS<sub>pp</sub> combination treatment is effective in multiple SCLC cell lines and in 1512-1A.

(A) Graphs show the sensitivity to TLS<sub>pp</sub> single agent (left) or OT + TLS<sub>pp</sub> combination (center and right) in SCLC cell lines indicated in Figure 7C-D and their neuroendocrine status. Statistical significance calculated by two-tailed Mann–Whitney test and p values are indicated in the figure. (B) Graph showing the correlation between sensitivity to OT and to OT + TLS<sub>pp</sub> in SCLC cell lines indicated in Figure 7C-D. Pearson correlation coefficients (*r*) and p values are indicated in the figure. (C) Kaplan Meier survival plot corresponding to experiment shown in Figure 7E-F. (D) Cell viability in the presence of different concentrations of TLS<sub>pp</sub>. Drug concentration is indicated data represent the mean percentages of survival from at least two independent experiments. (E) Cell survival assay with 1512-1A cells treated with OT at indicated concentrations, in the presence of TLS<sub>pp</sub> (blue, orange, and red curves) or without TLS<sub>pp</sub> (black curve). Left panel shows cell viability when treated with fixed concentration of olaparib and increasing concentration of TMZ. Right panel shows cell viability when treated with fixed concentration of TMZ and increasing concentration of olaparib. Data represent the mean percentages of survival from at least two independent experiments. Statistical analysis was calculated with one-way ANOVA Tukey multiple comparisons and all P values are described in the section “Statistical methods”. (F-G) Solid curves represent mean % initial tumor volume versus time (days) after either a single cycle (days 1-5) of TLS<sub>pp</sub> (100 mpk qd), OT (Ola 50 mpk bid + TMZ 25 mpk qd), or TLS<sub>pp</sub> + OT (F) or two cycles interspersed by three weeks of no treatment (G). Dashed curves represent tumor volume curve ± SEM. Number of replicate xenografts per regimen as represented parenthetically. Grayed area represents the treatment cycles. (H) Model for acquired chemoresistance mechanisms in SCLC. The presence of a subpopulation of cells in either G0 or G1 that can better tolerate DNA damage together with the increase activity of bypass polymerases, give an advantage to resistant tumors allowing them to survive after OT treatment. At the same time, damage bypass activity increases genome instability, and could provide additional mechanisms to avoid cell death after chemotherapy. This provides one likely, but not exclusive, mechanism for chemoresistance in SCLC.

## REFERENCES AND NOTES

1. J. George, J. S. Lim, S. J. Jang, Y. Cun, L. Ozretic, G. Kong, F. Leenders, X. Lu, L. Fernandez-Cuesta, G. Bosco, C. Muller, I. Dahmen, N. S. Jahchan, K. S. Park, D. Yang, A. N. Karnezis, D. Vaka, A. Torres, M. S. Wang, J. O. Korbel, R. Menon, S. M. Chun, D. Kim, M. Wilkerson, N. Hayes, D. Engelmann, B. Putzer, M. Bos, S. Michels, I. Vlastic, D. Seidel, B. Pinther, P. Schaub, C. Becker, J. Altmuller, J. Yokota, T. Kohno, R. Iwakawa, K. Tsuta, M. Noguchi, T. Muley, H. Hoffmann, P. A. Schnabel, I. Petersen, Y. Chen, A. Soltermann, V. Tischler, C. M. Choi, Y. H. Kim, P. P. Massion, Y. Zou, D. Jovanovic, M. Kontic, G. M. Wright, P. A. Russell, B. Solomon, I. Koch, M. Lindner, L. A. Muscarella, A. la Torre, J. K. Field, M. Jakopovic, J. Knezevic, E. Castanos-Velez, L. Roz, U. Pastorino, O. T. Brustugun, M. Lund-Iversen, E. Thunnissen, J. Kohler, M. Schuler, J. Botling, M. Sandelin, M. Sanchez-Cespedes, H. B. Salvesen, V. Achter, U. Lang, M. Bogus, P. M. Schneider, T. Zander, S. Ansen, M. Hallek, J. Wolf, M. Vingron, Y. Yatabe, W. D. Travis, P. Nurnberg, C. Reinhardt, S. Perner, L. Heukamp, R. Buttner, S. A. Haas, E. Brambilla, M. Peifer, J. Sage, R. K. Thomas, Comprehensive genomic profiles of small cell lung cancer. *Nature* **524**, 47–53 (2015).
2. C. M. Rudin, S. Durinck, E. W. Stawiski, J. T. Poirier, Z. Modrusan, D. S. Shames, E. A. Bergbower, Y. Guan, J. Shin, J. Guillory, C. S. Rivers, C. K. Foo, D. Bhatt, J. Stinson, F. Gnad, P. M. Haverty, R. Gentleman, S. Chaudhuri, V. Janakiraman, B. S. Jaiswal, C. Parikh, W. Yuan, Z. Zhang, H. Koeppen, T. D. Wu, H. M. Stern, R. L. Yauch, K. E. Huffman, D. D. Paskulin, P. B. Illei, M. Varella-Garcia, A. F. Gazdar, F. J. de Sauvage, R. Bourgon, J. D. Minna, M. V. Brock, S. Seshagiri, Comprehensive genomic analysis identifies SOX2 as a frequently amplified gene in small-cell lung cancer. *Nat. Genet.* **44**, 1111–1116 (2012).
3. M. Peifer, L. Fernandez-Cuesta, M. L. Sos, J. George, D. Seidel, L. H. Kasper, D. Plenker, F. Leenders, R. Sun, T. Zander, R. Menon, M. Koker, I. Dahmen, C. Muller, V. Di Cerbo, H. U. Schildhaus, J. Altmuller, I. Baessmann, C. Becker, B. de Wilde, J. Vandesompele, D. Bohm, S. Ansen, F. Gabler, I. Wilkening, S. Heynck, J. M. Heuckmann, X. Lu, S. L. Carter, K. Cibulskis, S. Banerji, G. Getz, K. S. Park, D. Rauh, C. Grutter, M. Fischer, L. Pasqualucci, G. Wright, Z. Wainer, P. Russell, I. Petersen, Y. Chen, E. Stoelben, C. Ludwig, P. Schnabel, H. Hoffmann, T. Muley, M. Brockmann, W. Engel-Riedel, L. A. Muscarella, V. M. Fazio, H. Groen, W. Timens, H. Sietsma, E. Thunnissen, E. Smit, D. A. Heideman, P. J. Snijders, F. Cappuzzo, C. Ligorio, S. Damiani, J. Field, S. Solberg, O. T. Brustugun, M. Lund-Iversen, J. Sanger, J. H. Clement, A. Soltermann, H. Moch, W. Weder, B. Solomon, J. C. Soria, P. Validire, B. Besse, E. Brambilla, C. Brambilla, S. Lantuejoul, P. Lorimier, P. M. Schneider, M. Hallek, W. Pao, M. Meyerson, J. Sage, J. Shendure, R. Schneider, R. Buttner, J. Wolf, P. Nurnberg, S. Perner, L. C. Heukamp, P. K. Brindle, S. Haas, R. K. Thomas, Integrative genome analyses identify key somatic driver mutations of small-cell lung cancer. *Nat. Genet.* **44**, 1104–1110 (2012).
4. L. Horn, A. S. Mansfield, A. Szczesna, L. Havel, M. Krzakowski, M. J. Hochmair, F. Huemer, G. Losonczy, M. L. Johnson, M. Nishio, M. Reck, T. Mok, S. Lam, D. S. Shames, J. Liu, B. Ding, A. Lopez-Chavez, F. Kabbinar, W. Lin, A. Sandler, S. V. Liu, First-line atezolizumab plus chemotherapy in extensive-stage small-cell lung cancer. *N. Engl. J. Med.* **379**, 2220–2229 (2018).

5. L. Paz-Ares, M. Dvorkin, Y. Chen, N. Reinmuth, K. Hotta, D. Trukhin, G. Statsenko, M. J. Hochmair, M. Özgüroğlu, J. H. Ji, O. Voitko, A. Poltoratskiy, S. Ponce, F. Verderame, L. Havel, I. Bondarenko, A. Kazarnowicz, G. Losonczy, N. V. Conev, J. Armstrong, N. Byrne, N. Shire, H. Jiang, J. W. Goldman; CASPIAN Investigators, Durvalumab plus platinum-etoposide versus platinum-etoposide in first-line treatment of extensive-stage small-cell lung cancer (CASPIAN): A randomised, controlled, open-label, phase 3 trial. *Lancet* **394**, 1929–1939 (2019).
6. M. Santarpià, M. G. Daffina, N. Karachaliou, M. Gonzalez-Cao, C. Lazzari, G. Altavilla, R. Rosell, Targeted drugs in small-cell lung cancer. *Transl. Lung Cancer Res.* **5**, 51–70 (2016).
7. L. A. Byers, C. M. Rudin, Small cell lung cancer: Where do we go from here? *Cancer* **121**, 664–672 (2015).
8. E. Shtivelman, T. Hensing, G. R. Simon, P. A. Dennis, G. A. Otterson, R. Bueno, R. Salgia, Molecular pathways and therapeutic targets in lung cancer. *Oncotarget* **5**, 1392–1433 (2014).
9. A. F. Farago, F. K. Keane, Current standards for clinical management of small cell lung cancer. *Transl. Lung Cancer Res.* **7**, 69–79 (2018).
10. D. S. Ettinger, D. E. Wood, D. L. Aisner, W. Akerley, J. R. Bauman, A. Bharat, D. S. Bruno, J. Y. Chang, L. R. Chirieac, T. A. D'Amico, T. J. Dilling, J. Dowell, S. Gettinger, M. A. Gubens, A. Hegde, M. Hennon, R. P. Lackner, M. Lanuti, T. A. Leal, J. Lin, B. W. Loo, Jr., C. M. Lovly, R. G. Martins, E. Massarelli, D. Morgensztern, T. Ng, G. A. Otterson, S. P. Patel, G. J. Riely, S. E. Schild, T. A. Shapiro, A. P. Singh, J. Stevenson, A. Tam, J. Yanagawa, S. C. Yang, K. M. Gregory, M. Hughes, NCCN guidelines insights: Non-small cell lung cancer, version 2.2021. *J. Natl. Compr. Canc. Netw.* **19**, 254–266 (2021).
11. T. S. Mok, Y. L. Wu, S. Thongprasert, C. H. Yang, D. T. Chu, N. Saijo, P. Sunpaweravong, B. Han, B. Margono, Y. Ichinose, Y. Nishiwaki, Y. Ohe, J. J. Yang, B. Chewaskulyong, H. Jiang, E. L. Duffield, C. L. Watkins, A. A. Armour, M. Fukuoka, Gefitinib or carboplatin-paclitaxel in pulmonary adenocarcinoma. *N. Engl. J. Med.* **361**, 947–957 (2009).
12. T. S. Mok, Y. L. Wu, M. J. Ahn, M. C. Garassino, H. R. Kim, S. S. Ramalingam, F. A. Shepherd, Y. He, H. Akamatsu, W. S. Theelen, C. K. Lee, M. Sebastian, A. Templeton, H. Mann, M. Marotti, S. Ghiorghiu, V. A. Papadimitrakopoulou; AURA3 Investigators, Osimertinib or platinum-pemetrexed in EGFR T790M-positive lung cancer. *N. Engl. J. Med.* **376**, 629–640 (2017).
13. W. Pao, V. A. Miller, K. A. Politi, G. J. Riely, R. Somwar, M. F. Zakowski, M. G. Kris, H. Varmus, Acquired resistance of lung adenocarcinomas to gefitinib or erlotinib is associated with a second mutation in the EGFR kinase domain. *PLOS Med.* **2**, e73 (2005).
14. S. Kobayashi, T. J. Boggon, T. Dayaram, P. A. Janne, O. Kocher, M. Meyerson, B. E. Johnson, M. J. Eck, D. G. Tenen, B. Halmos, EGFR mutation and resistance of non-small-cell lung cancer to gefitinib. *N. Engl. J. Med.* **352**, 786–792 (2005).
15. L. V. Sequist, B. A. Waltman, D. Dias-Santagata, S. Digumarthy, A. B. Turke, P. Fidias, K. Bergethon, A. T. Shaw, S. Gettinger, A. K. Cosper, S. Akhavanfard, R. S. Heist, J. Temel, J. G.

Christensen, J. C. Wain, T. J. Lynch, K. Vernovsky, E. J. Mark, M. Lanuti, A. J. Iafrate, M. Mino-Kenudson, J. A. Engelman, Genotypic and histological evolution of lung cancers acquiring resistance to EGFR inhibitors. *Sci. Transl. Med.* **3**, 75ra26 (2011).

16. Z. Piotrowska, H. Isozaki, J. K. Lennerz, J. F. Gainor, I. T. Lennes, V. W. Zhu, N. Marcoux, M. K. Banwait, S. R. Digumarthy, W. Su, S. Yoda, A. K. Riley, V. Nangia, J. J. Lin, R. J. Nagy, R. B. Lanman, D. Dias-Santagata, M. Mino-Kenudson, A. J. Iafrate, R. S. Heist, A. T. Shaw, E. K. Evans, C. Clifford, S. I. Ou, B. Wolf, A. N. Hata, L. V. Sequist, Landscape of acquired resistance to osimertinib in *EGFR*-mutant NSCLC and clinical validation of combined EGFR and RET inhibition with osimertinib and BLU-667 for acquired *RET* Fusion. *Cancer Discov.* **8**, 1529–1539 (2018).

17. S. E. Mirski, J. H. Gerlach, S. P. Cole, Multidrug resistance in a human small cell lung cancer cell line selected in adriamycin. *Cancer Res.* **47**, 2594–2598 (1987).

18. P. R. Twentyman, K. A. Wright, P. Mistry, L. R. Kelland, B. A. Murrer, Sensitivity to novel platinum compounds of panels of human lung cancer cell lines with acquired and inherent resistance to cisplatin. *Cancer Res.* **52**, 5674–5680 (1992).

19. E. E. Gardner, B. H. Lok, V. E. Schneeberger, P. Desmeules, L. A. Miles, P. K. Arnold, A. Ni, I. Khodos, E. de Stanchina, T. Nguyen, J. Sage, J. E. Campbell, S. Ribich, N. Rekhtman, A. Dowlati, P. P. Massion, C. M. Rudin, J. T. Poirier, Chemosensitive relapse in small cell lung cancer proceeds through an EZH2-SLFN11 axis. *Cancer Cell* **31**, 286–299 (2017).

20. F. Böttger, E. A. Semenova, J.-Y. Song, G. Ferone, J. van der Vliet, M. Cozijnsen, R. Bhaskaran, L. Bombardelli, S. R. Piersma, T. V. Pham, C. R. Jimenez, A. Berns, Tumor heterogeneity underlies differential cisplatin sensitivity in mouse models of small-cell lung cancer. *Cell Rep.* **27**, 3345–3358.e4 (2019).

21. B. J. Drapkin, J. George, C. L. Christensen, M. Mino-Kenudson, R. Dries, T. Sundaresan, S. Phat, D. T. Myers, J. Zhong, P. Igo, M. H. Hazar-Rethinam, J. A. Licausi, M. Gomez-Caraballo, M. Kem, K. N. Jani, R. Azimi, N. Abedpour, R. Menon, S. Lakis, R. S. Heist, R. Buttner, S. Haas, L. V. Sequist, A. T. Shaw, K. K. Wong, A. N. Hata, M. Toner, S. Maheswaran, D. A. Haber, M. Peifer, N. Dyson, R. K. Thomas, A. F. Farago, Genomic and functional fidelity of small cell lung cancer patient-derived xenografts. *Cancer Discov.* **8**, 600–615 (2018).

22. C. L. Hodgkinson, C. J. Morrow, Y. Li, R. L. Metcalf, D. G. Rothwell, F. Trapani, R. Polanski, D. J. Burt, K. L. Simpson, K. Morris, S. D. Pepper, D. Nonaka, A. Greystoke, P. Kelly, B. Bola, M. G. Krebs, J. Antonello, M. Ayub, S. Faulkner, L. Priest, L. Carter, C. Tate, C. J. Miller, F. Blackhall, G. Brady, C. Dive, Tumorigenicity and genetic profiling of circulating tumor cells in small-cell lung cancer. *Nat. Med.* **20**, 897–903 (2014).

23. J. A. Williams, Using PDX for preclinical cancer drug discovery: The evolving field. *J. Clin. Med.* **7**, 41 (2018).

24. V. Vidhyasagar, S. U. Haq, B. H. Lok, Patient-derived xenograft models of small cell lung cancer for therapeutic development. *Clin. Oncol. (R. Coll. Radiol.)* **32**, 619–625 (2020).

25. A. F. Farago, B. Y. Yeap, M. Stanzione, Y. P. Hung, R. S. Heist, J. P. Marcoux, J. Zhong, D. Rangachari, D. A. Barbie, S. Phat, D. T. Myers, R. Morris, M. Kem, T. D. Dubash, E. A. Kennedy, S. R. Digumarthy, L. V. Sequist, A. N. Hata, S. Maheswaran, D. A. Haber, M. S. Lawrence, A. T. Shaw, M. Mino-Kenudson, N. J. Dyson, B. J. Drapkin, Combination olaparib and temozolomide in relapsed small-cell lung cancer. *Cancer Discov.* **9**, 1372–1387 (2019).
26. M. C. Pietanza, S. N. Waqar, L. M. Krug, A. Dowlati, C. L. Hann, A. Chiappori, T. K. Owonikoko, K. M. Woo, R. J. Cardnell, J. Fujimoto, L. Long, L. Diao, J. Wang, Y. Bensman, B. Hurtado, P. de Groot, E. P. Sulman, I. I. Wistuba, A. Chen, M. Fleisher, J. V. Heymach, M. G. Kris, C. M. Rudin, L. A. Byers, Randomized, double-blind, phase II study of temozolomide in combination with either veliparib or placebo in patients with relapsed-sensitive or refractory small-cell lung cancer. *J. Clin. Oncol.* **36**, 2386–2394 (2018).
27. J. Doles, T. G. Oliver, E. R. Cameron, G. Hsu, T. Jacks, G. C. Walker, M. T. Hemann, Suppression of Rev3, the catalytic subunit of Pol{zeta}, sensitizes drug-resistant lung tumors to chemotherapy. *Proc. Natl. Acad. Sci. U.S.A.* **107**, 20786–20791 (2010).
28. K. Xie, J. Doles, M. T. Hemann, G. C. Walker, Error-prone translesion synthesis mediates acquired chemoresistance. *Proc. Natl. Acad. Sci. U.S.A.* **107**, 20792–20797 (2010).
29. S. L. Gerson, MGMT: Its role in cancer aetiology and cancer therapeutics. *Nat. Rev. Cancer* **4**, 296–307 (2004).
30. J. L. Munoz, N. D. Walker, K. W. Scotto, P. Rameshwar, Temozolomide competes for P-glycoprotein and contributes to chemoresistance in glioblastoma cells. *Cancer Lett.* **367**, 69–75 (2015).
31. F. J. Sharom, ABC multidrug transporters: Structure, function and role in chemoresistance. *Pharmacogenomics* **9**, 105–127 (2008).
2. J. Murai, S. W. Tang, E. Leo, S. A. Baechler, C. E. Redon, H. Zhang, M. Al Abo, V. N. Rajapakse, E. Nakamura, L. M. M. Jenkins, M. I. Aladjem, Y. Pommier, SLFN11 blocks stressed replication forks independently of ATR. *Mol. Cell* **69**, 371–384.e6 (2018).
33. B. H. Lok, E. E. Gardner, V. E. Schneeberger, A. Ni, P. Desmeules, N. Rekhman, E. de Stanchina, B. A. Teicher, N. Riaz, S. N. Powell, J. T. Poirier, C. M. Rudin, PARP inhibitor activity correlates with SLFN11 expression and demonstrates synergy with temozolomide in small cell lung cancer. *Clin. Cancer Res.* **23**, 523–535 (2017).
4. G. Zoppoli, M. Regairaz, E. Leo, W. C. Reinhold, S. Varma, A. Ballestrero, J. H. Doroshow, Y. Pommier, Putative DNA/RNA helicase Schlafen-11 (SLFN11) sensitizes cancer cells to DNA-damaging agents. *Proc. Natl. Acad. Sci. U.S.A.* **109**, 15030–15035 (2012).
35. P. L. Olive, D. Wlodek, J. P. Banath, DNA double-strand breaks measured in individual cells subjected to gel electrophoresis. *Cancer Res.* **51**, 4671–4676 (1991).
36. A. Marechal, L. Zou, DNA damage sensing by the ATM and ATR kinases. *Cold Spring Harb. Perspect. Biol.* **5** (2013).

37. X. Sun, P. D. Kaufman, Ki-67: More than a proliferation marker. *Chromosoma* **127**, 175–186 (2018).
38. S. Tada, Cdt1 and geminin: Role during cell cycle progression and DNA damage in higher eukaryotes. *Front. Biosci.* **12**, 1629–1641 (2007).
39. Y. Hao, S. Hao, E. Andersen-Nissen, W. M. Mauck III, S. Zheng, A. Butler, M. J. Lee, A. J. Wilk, C. Darby, M. Zager, P. Hoffman, M. Stoeckius, E. Papalexi, E. P. Mimitou, J. Jain, A. Srivastava, T. Stuart, L. M. Fleming, B. Yeung, A. J. Rogers, J. M. McElrath, C. A. Blish, R. Gottardo, P. Smibert, R. Satija, Integrated analysis of multimodal single-cell data. *Cell* **184**, 3573–3587.e29 (2021).
40. J. Murai, Y. Zhang, J. Morris, J. Ji, S. Takeda, J. H. Doroshov, Y. Pommier, Rationale for poly(ADP-ribose) polymerase (PARP) inhibitors in combination therapy with camptothecins or temozolomide based on PARP trapping versus catalytic inhibition. *J. Pharmacol. Exp. Ther.* **349**, 408–416 (2014).
41. K. Yoshimoto, M. Mizoguchi, N. Hata, H. Murata, R. Hatae, T. Amano, A. Nakamizo, T. Sasaki, Complex DNA repair pathways as possible therapeutic targets to overcome temozolomide resistance in glioblastoma. *Front. Oncol.* **2**, 186 (2012).
42. A. Vaisman, R. Woodgate, Translesion DNA polymerases in eukaryotes: What makes them tick? *Crit. Rev. Biochem. Mol. Biol.* **52**, 274–303 (2017).
43. N. Chatterjee, G. C. Walker, Mechanisms of DNA damage, repair, and mutagenesis. *Environ. Mol. Mutagen.* **58**, 235–263 (2017).
44. G. Maga, E. Crespan, E. Markkanen, R. Imhof, A. Furrer, G. Villani, U. Hubscher, B. van Loon, DNA polymerase  $\delta$ -interacting protein 2 is a processivity factor for DNA polymerase  $\lambda$  during 8-oxo-7,8-dihydroguanine bypass. *Proc. Natl. Acad. Sci. U.S.A.* **110**, 18850–18855 (2013).
45. T. A. Guillian, L. J. Bailey, N. C. Brissett, A. J. Doherty, PolDIP2 interacts with human PrimPol and enhances its DNA polymerase activities. *Nucleic Acids Res.* **44**, 3317–3329 (2016).
46. Y. S. Lee, M. T. Gregory, W. Yang, Human Pol  $\zeta$  purified with accessory subunits is active in translesion DNA synthesis and complements Pol  $\eta$  in cisplatin bypass. *Proc. Natl. Acad. Sci. U.S.A.* **111**, 2954–2959 (2014).
47. A. Maya-Mendoza, P. Moudry, J. M. Merchut-Maya, M. Lee, R. Strauss, J. Bartek, High speed of fork progression induces DNA replication stress and genomic instability. *Nature* **559**, 279–284 (2018).
48. S. Avkin, Z. Sevilya, L. Toubé, N. Geacintov, S. G. Chaney, M. Oren, Z. Livneh, p53 and p21 regulate error-prone DNA repair to yield a lower mutation load. *Mol. Cell* **22**, 407–413 (2006).
49. D. M. Korzhnev, M. K. Hadden, Targeting the translesion synthesis pathway for the development of anti-cancer chemotherapeutics. *J. Med. Chem.* **59**, 9321–9336 (2016).



50. R. C. Dash, Z. Ozen, A. A. Rizzo, S. Lim, D. M. Korzhnev, M. K. Hadden, Structural approach to identify a lead scaffold that targets the translesion synthesis polymerase Rev1. *J. Chem. Inf. Model.* **58**, 2266–2277 (2018).
51. N. Chatterjee, M. A. Whitman, C. A. Harris, S. M. Min, O. Jonas, E. C. Lien, A. Luengo, M. G. Vander Heiden, J. Hong, P. Zhou, M. T. Hemann, G. C. Walker, REV1 inhibitor JH-RE-06 enhances tumor cell response to chemotherapy by triggering senescence hallmarks. *Proc. Natl. Acad. Sci. U.S.A.* **117**, 28918–28921 (2020).
52. J. L. Wojtaszek, N. Chatterjee, J. Najeeb, A. Ramos, M. Lee, K. Bian, J. Y. Xue, B. A. Fenton, H. Park, D. Li, M. T. Hemann, J. Hong, G. C. Walker, P. Zhou, A small molecule targeting mutagenic translesion synthesis improves chemotherapy. *Cell* **178**, 152–159.e111 (2019).
53. S. Nayak, J. A. Calvo, K. Cong, M. Peng, E. Berthiaume, J. Jackson, A. M. Zaino, A. Vindigni, M. K. Hadden, S. B. Cantor, Inhibition of the translesion synthesis polymerase REV1 exploits replication gaps as a cancer vulnerability. *Sci. Adv.* **6**, eaaz7808 (2020).
54. B. H. Herzog, S. Devarakonda, R. Govindan, Overcoming chemotherapy resistance in SCLC. *J. Thorac. Oncol.* **16**, 2002–2015 (2021).
55. S. M. Noordermeer, H. van Attikum, PARP inhibitor resistance: A tug-of-war in BRCA-mutated cells. *Trends Cell Biol.* **29**, 820–834 (2019).
56. K. Suda, I. Murakami, K. Sakai, K. Tomizawa, H. Mizuuchi, K. Sato, K. Nishio, T. Mitsudomi, Heterogeneity in resistance mechanisms causes shorter duration of epidermal growth factor receptor kinase inhibitor treatment in lung cancer. *Lung Cancer* **91**, 36–40 (2016).
57. Z. Piotrowska, M. J. Niederst, C. A. Karlovich, H. A. Wakelee, J. W. Neal, M. Mino-Kenudson, L. Fulton, A. N. Hata, E. L. Lockerman, A. Kalsy, S. Digumarthy, A. Muzikansky, M. Raponi, A. R. Garcia, H. E. Mulvey, M. K. Parks, R. H. DiCecca, D. Dias-Santagata, A. J. Iafrate, A. T. Shaw, A. R. Allen, J. A. Engelman, L. V. Sequist, Heterogeneity underlies the emergence of EGFR T790M wild-type clones following treatment of T790M-positive cancers with a third-generation EGFR inhibitor. *Cancer Discov.* **5**, 713–722 (2015).
58. K. Suda, I. Murakami, T. Katayama, K. Tomizawa, H. Osada, Y. Sekido, Y. Maehara, Y. Yatabe, T. Mitsudomi, Reciprocal and complementary role of MET amplification and EGFR T790M mutation in acquired resistance to kinase inhibitors in lung cancer. *Clin. Cancer Res.* **16**, 5489–5498 (2010).
59. K. Suda, I. Murakami, K. Sakai, H. Mizuuchi, S. Shimizu, K. Sato, K. Tomizawa, S. Tomida, Y. Yatabe, K. Nishio, T. Mitsudomi, Small cell lung cancer transformation and T790M mutation: Complementary roles in acquired resistance to kinase inhibitors in lung cancer. *Sci. Rep.* **5**, 14447 (2015).
60. D. Fu, J. A. Calvo, L. D. Samson, Balancing repair and tolerance of DNA damage caused by alkylating agents. *Nat. Rev. Cancer* **12**, 104–120 (2012).

61. W. Roos, M. Baumgartner, B. Kaina, Apoptosis triggered by DNA damage O6-methylguanine in human lymphocytes requires DNA replication and is mediated by p53 and Fas/CD95/Apo-1. *Oncogene* **23**, 359–367 (2004).
62. F. Wu, X. Lin, T. Okuda, S. B. Howell, DNA polymerase zeta regulates cisplatin cytotoxicity, mutagenicity, and the rate of development of cisplatin resistance. *Cancer Res.* **64**, 8029–8035 (2004).
63. W. P. Roos, A. Tsaalbi-Shtylik, R. Tsaryk, F. Guvercin, N. de Wind, B. Kaina, The translesion polymerase Rev3L in the tolerance of alkylating anticancer drugs. *Mol. Pharmacol.* **76**, 927–934 (2009).
64. Y. Sakurai, M. Ichinoe, K. Yoshida, Y. Nakazato, S. Saito, M. Satoh, N. Nakada, I. Sanoyama, A. Umezawa, Y. Numata, J. Shi-Xu, M. Ichihara, M. Takahashi, Y. Murakumo, Inactivation of REV7 enhances chemosensitivity and overcomes acquired chemoresistance in testicular germ cell tumors. *Cancer Lett.* **489**, 100–110 (2020).
65. S. Nayak, J. A. Calvo, S. B. Cantor, Targeting translesion synthesis (TLS) to expose replication gaps, a unique cancer vulnerability. *Expert Opin. Ther. Targets* **25**, 27–36 (2021).
66. T. Okuda, X. Lin, J. Trang, S. B. Howell, Suppression of hREV1 expression reduces the rate at which human ovarian carcinoma cells acquire resistance to cisplatin. *Mol. Pharmacol.* **67**, 1852–1860 (2005).
67. H. Chen, H. Chen, J. Zhang, Y. Wang, A. Simoneau, H. Yang, A. S. Levine, L. Zou, Z. Chen, L. Lan, cGAS suppresses genomic instability as a decelerator of replication forks. *Sci. Adv.* **6**, eabb8941 (2020).
68. H. A. Collier, C. Grandori, P. Tamayo, T. Colbert, E. S. Lander, R. N. Eisenman, T. R. Golub, Expression analysis with oligonucleotide microarrays reveals that MYC regulates genes involved in growth, cell cycle, signaling, and adhesion. *Proc. Natl. Acad. Sci. U.S.A.* **97**, 3260–3265 (2000).
69. A. L. Gartel, X. Ye, E. Goufman, P. Shianov, N. Hay, F. Najmabadi, A. L. Tyner, Myc represses the p21(WAF1/CIP1) promoter and interacts with Sp1/Sp3. *Proc. Natl. Acad. Sci. U.S.A.* **98**, 4510–4515 (2001).
70. H. Li, R. Durbin, Fast and accurate short read alignment with Burrows-Wheeler transform. *Bioinformatics* **25**, 1754–1760 (2009).
1. K. Cibulskis, M. S. Lawrence, S. L. Carter, A. Sivachenko, D. Jaffe, C. Sougnez, S. Gabriel, M. Meyerson, E. S. Lander, G. Getz, Sensitive detection of somatic point mutations in impure and heterogeneous cancer samples. *Nat. Biotechnol.* **31**, 213–219 (2013).
72. S. Kim, K. Scheffler, A. L. Halpern, M. A. Bekritsky, E. Noh, M. Källberg, X. Chen, Y. Kim, D. Beyter, P. Krusche, C. T. Saunders, Strelka2: Fast and accurate calling of germline and somatic variants. *Nat. Methods* **15**, 591–594 (2018).

73. B. K. Mannakee, U. Balaji, A. K. Witkiewicz, R. N. Gutenkunst, E. S. Knudsen, Sensitive and specific post-call filtering of genetic variants in xenograft and primary tumors. *Bioinformatics* **34**, 1713–1718 (2018).
74. P. Cingolani, A. Platts, L. Wang le, M. Coon, T. Nguyen, L. Wang, S. J. Land, X. Lu, D. M. Ruden, A program for annotating and predicting the effects of single nucleotide polymorphisms, SnpEff: SNPs in the genome of *Drosophila melanogaster* strain w1118; iso-2; iso-3. *Fly* **6**, 80–92 (2012).
75. R. Shen, V. E. Seshan, FACETS: Allele-specific copy number and clonal heterogeneity analysis tool for high-throughput DNA sequencing. *Nucleic Acids Res.* **44**, e131 (2016).
76. J. J. Lin, A. Langenbucher, P. Gupta, S. Yoda, I. J. Fetter, M. Rooney, A. Do, M. Kem, K. P. Chang, A. Y. Oh, E. Chin, D. Juric, R. B. Corcoran, I. Dagogo-Jack, J. F. Gainor, J. R. Stone, J. K. Lennerz, M. S. Lawrence, A. N. Hata, M. Mino-Kenudson, A. T. Shaw, Small cell transformation of *ROS1* fusion-positive lung cancer resistant to ROS1 inhibition. *npj Precis. Oncol.* **4**, 21 (2020).
77. R. J. C. Kluin, K. Kemper, T. Kuilman, J. R. de Rooter, V. Iyer, J. V. Forment, P. Cornelissen-Steijger, I. de Rink, P. Ter Brugge, J. Y. Song, S. Klarenbeek, U. McDermott, J. Jonkers, A. Velds, D. J. Adams, D. S. Peeper, O. Krijgsman, Xenofilter: Computational deconvolution of mouse and human reads in tumor xenograft sequence data. *BMC Bioinformatics* **19**, 366 (2018).
78. C. McQuin, A. Goodman, V. Chernyshev, L. Kametsky, B. A. Cimini, K. W. Karhohs, M. Doan, L. Ding, S. M. Rafelski, D. Thirstrup, W. Wiegraeb, S. Singh, T. Becker, J. C. Caicedo, A. E. Carpenter, CellProfiler 3.0: Next-generation image processing for biology. *PLOS Biol.* **16**, e2005970 (2018).
9. M. M. Genois, J. P. Gagne, T. Yasuhara, J. Jackson, S. Saxena, M. F. Langelier, I. Ahel, M. T. Bedford, J. M. Pascal, A. Vindigni, G. G. Poirier, L. Zou, CARM1 regulates replication fork speed and stress response by stimulating PARP1. *Mol. Cell* **81**, 784–800.e8 (2021).
80. P. L. Olive, J. P. Banath, The comet assay: A method to measure DNA damage in individual cells. *Nat. Protoc.* **1**, 23–29 (2006).
81. B. M. Gyori, G. Venkatachalam, P. S. Thiagarajan, D. Hsu, M. V. Clement, OpenComet: An automated tool for comet assay image analysis. *Redox Biol.* **2**, 457–465 (2014).
82. J. G. Tate, S. Bamford, H. C. Jubb, Z. Sondka, D. M. Beare, N. Bindal, H. Boutselakis, C. G. Cole, C. Creatore, E. Dawson, P. Fish, B. Harsha, C. Hathaway, S. C. Jupe, C. Y. Kok, K. Noble, L. Ponting, C. C. Ramshaw, C. E. Rye, H. E. Speedy, R. Stefancsik, S. L. Thompson, S. Wang, S. Ward, P. J. Campbell, S. A. Forbes, COSMIC: The catalogue of somatic mutations in cancer. *Nucleic Acids Res.* **47**, D941–D947 (2019).
83. C. J. Lord, A. Ashworth, BRCAness revisited. *Nat. Rev. Cancer* **16**, 110–120 (2016).